

Combined Impact of Joule Heating, Activation Energy, and Viscous Dissipation on Ternary Nanofluid Flow over Three Different Geometries



Kandavkovi Mallikarjuna Nihaal¹, Ulavathi Shettar Mahabaleshwar¹, Sang Woo Joo², Giulio Lorenzini^{3*}

¹ Department of Studies in Mathematics, Davangere University, Shivagangothri, Davangere 577 007, India

² School of Mechanical Engineering, Yeungnam University, Gyeongsan 38541, Korea

³ Department of Engineering and Architecture, Parco Area delle Scienze 181/A, Parma 43124, Italy

Corresponding Author Email: giulio.lorenzini@unipr.it

Copyright: ©2023 IIETA. This article is published by IIETA and is licensed under the CC BY 4.0 license (<http://creativecommons.org/licenses/by/4.0/>).

<https://doi.org/10.18280/ijcmem.110407>

ABSTRACT

Received: 28 September 2023

Revised: 7 November 2023

Accepted: 21 November 2023

Available online: 30 December 2023

Keywords:

ternary nanofluid, MHD, Joule heating, viscous heating, activation energy

Heat and mass transfer in ternary nanofluid flows over diverse geometries is particularly significant for thermal management in electronic devices, precipitation, and filtration. Chemical reactions are vital processes that occur in a variety of natural and industrial systems. With this initiation, this research explores the impacts of chemical reaction and heat source/sink over MHD ternary nano fluid flow. In addition to this model, we assessed joule heating, viscous dissipation, and activation energy for the study. The ODEs are obtained by using appropriate similarities and the altered non-linear governing equations are solved numerically utilizing RKF-45 and shooting technique. The influence of vital variables on common profiles (flow velocity, thermal gradient, and mass transmission rate) is explored and deliberated graphically in three distinct scenarios. When compared to the other scenarios, the mass transfer for the case of fluid flow across a plate lowers as the activation energy parameter goes up.

1. INTRODUCTION

To continue exploring nanofluids, scientists have introduced the concept of a ternary nanofluid, which is a mixture of various nanoparticles with the conventional fluid. The ternary nanofluid's main benefit is to further improve heat transmission properties. In terms of energy exchange, ternary nanofluid beats regular fluids, nanofluid, hybrid nanofluid, petrol, and methanol. Because of their increased thermal conductivity and heat transfer capabilities over conventional nanofluids, ternary nanofluids have piqued the interest of scientists and researchers looking for new opportunities in these applications such as electrical gadget cooling, nuclear plants, automotives, and refrigerators. Recent advances in the research field using ternary nanofluid can be found in Abbasi and Ashraf [1], Animasaun et al. [2], Maranna et al. [3], and Alanazi et al. [4].

The significance of magnetic field and porous medium effects on velocity and temperature field is crucial when it comes to astrophysics, petroleum, and material science areas. Gamiel et al. [5] investigated the effects of the porous media and magnetic field on the fibre cylindrical beds. An effective medium approximation has been used to investigate the total bed permeability (OBP). Fetecau and Moroşanu [6] investigated the combined effect of porous and magnetic fields on stable Second-grade fluid over an infinite plate. The author has examined two motion problems of some different types of fluids when velocity or shear stress is placed on the frontier. Manjunatha et al. [7] explored the effects of the triple diffusive

Marangoni convection (TDMC) problem in a fluid with porous structured layers. Mahabaleshwar et al. [8] evaluated the impact of Dufour and Soret on radioactive non-Newtonian fluid with MHD and mixed convection over a permeable sheet. Aslani et al. [9] scrutinized the mixed implication of radiation and inclined MHD on a Micropolar fluid over a perforated stretching/shrinking surface with Mass transpiration.

Joule heating is the process of producing heat by passing an electric current through a conductor. It has a substantial effect on the flow and heat transfer characteristics of fluids. It is crucial in the investigation of magnetohydrodynamic (MHD) flow [10, 11]. Joule heating possesses many industrial applications such as iron cooking, electric heaters, resistance ovens, and foodstuffs. Yashkun et al. [12] investigated the flow and heat transmission of a hybrid nanofluid on an exponentially changing sheet. In addition, the phenomena of mixed convection and joule heating in HNF were investigated. Khashi'ié et al. [13] researched the effect of Joule heating on MHD boundary layer flow of HNF over a mobile plate. They pointed out that a boost in the suction parameter and magnetic strength accelerates heat transfer. Sajid et al. [14] conducted a pioneering study on the impact of the modified innovative tetra hybrid Tiwari and Das nanofluid model on blood flow in the arteries. Cross non-Newtonian fluid model was considered. This article mainly focuses on heat transfer enhancements under the impacts of HSS, viscous dissipation, and joule heating.

Though fluid is very viscous, significant heat can be created even at very moderate speeds, such as in plastic extrusion,

lubrication, and viscometry, and so heat transfer results may vary significantly due to viscous dissipation. It is the irreversible process by which the work done by a fluid on adjacent layers due to the action of shear forces gets transformed into heat. Vajravelu and Hadjinicolaou [15] conducted an analysis of the heat transmission properties of a viscous fluid in the laminar boundary layer over a stretched surface, focusing on the effects of frictional heating (viscous heating) and HSS. Chen [16] investigated the effects of viscous dissipation on convective heat transmission in a non-Newtonian liquid layer over an unstable stretched sheet. They emphasized how the wall temperature gradient varies for different Eckert numbers. In the existence of radiation and viscous dissipation, Mahesh et al. [17] obtained a dual solution for MHD couple stress hybrid nanofluid flow over permeable surface. Hassan et al. [18] obtained an exact solution for 2-D radioactive MHD Casson fluid flow with first-order chemical reaction under the impact of viscous dissipation and HSS. Masood et al. [19] explored the characteristics of viscous dissipation in MHD nanofluid flow over stretched surface. To address nanoparticle transport, the author used Brownian diffusion and the thermophoresis phenomena.

Chemical reactions are used in the production of food, fibre insulation, ceramics and polymer production, fog formation, geo-thermal reservoirs, hydro-metallurgical industries, nuclear reactor cooling, and thermal oil recovery among other things. Except in spite of a catalyst, some reactions have been known to move slowly or don't move at all. Thus, in order to activate a chemical reaction, a minimum amount of energy, known as activation energy, is necessary. Activation energy is crucial in increasing the rate of chemical processes. The effect of nonlinear thermal radiation over Carreau nanofluid flow on stagnation point past a nonlinear stretched surface was investigated by Zaib et al. [20]. They considered activation energy and binary chemical reactions to analyze mass transfer analysis. Mustafa et al. [21] carried out the investigation of the mixed convective nanofluid flow with MHD past a vertical stretching sheet. Aspects of activation energy and chemical reaction were the main highlights. Some recent studies related to the various investigations over activation energy are found in the studies [22-24].

The goal of the current work is to study the physical significance of porous medium, magnetic field, and viscous dissipation over an incompressible flow ternary nanofluid past plate, cone, and wedge in the existence of activation energy and joule heating that has not been studied previously. Suitable similarities are employed to solve the system of non-linear PDEs to nonlinear ODEs. The impact of key factors on flow properties is explored and portrayed via graphs.

2. MATHEMATICAL MODEL

The present analysis considers three different geometries plate, cone, and wedge in which a two-dimensional, steady, incompressible ternary nanofluid is examined under the influence of MHD, porous media, and activation energy. Additionally, joule heating and viscous dissipation are considered. The current problem is considered in such a way that x axis is parallel to body's surface and y being normal. The physical model of the flow problem is shown in Figure 1. Let the half-angle of the cone/wedge, radius of the cone, and full angle of the wedge is symbolized as (γ, r, Θ) respectively.

The temperature nearby surface i.e., $(y = 0)$ and far-field temperature i.e., $(y \rightarrow \infty)$ is represented as (T_w, T_∞) . (C_w, C_∞) represents the concentration near the surface i.e., $(y = 0)$ and at far-field i.e., $(y \rightarrow \infty)$ representing boundary conditions.

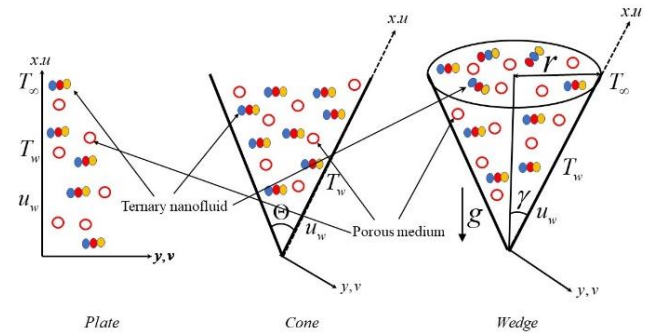


Figure 1. Flow geometry of the problem

Under the aforementioned assumptions, for the current flow problem the governing equations are as follows [25-27]:

$$\frac{\partial(r^m u)}{\partial x} + \frac{\partial(r^m v)}{\partial y} = 0 \quad (1)$$

$$u \frac{\partial u}{\partial x} + v \frac{\partial u}{\partial y} = v_{tnf} \frac{\partial^2 u}{\partial y^2} + \frac{g \rho_f (T - T_\infty) \varepsilon_T \cos \gamma}{\rho_{tnf}} - v_{tnf} \frac{u}{K^*} - \frac{\sigma_{tnf}}{\rho_{tnf}} B_0^2 u \quad (2)$$

$$u \frac{\partial T}{\partial x} + v \frac{\partial T}{\partial y} = \frac{k_{tnf}}{(\rho C_p)_{tnf}} \frac{\partial^2 T}{\partial y^2} + \frac{\mu_{tnf}}{(\rho C_p)_{tnf}} \left(\frac{\partial u}{\partial y} \right)^2 + \frac{\sigma_{tnf}}{(\rho C_p)_{tnf}} B_0^2 u^2 + \frac{Q}{(\rho C_p)_{tnf}} (T - T_\infty) \quad (3)$$

$$u \frac{\partial C}{\partial x} + v \frac{\partial C}{\partial y} = D_B \frac{\partial^2 C}{\partial y^2} - k_r^2 \left(\frac{T}{T_\infty} \right)^n - e^{-\frac{E_a}{KT}} (C - C_\infty) \quad (4)$$

The relevant boundary conditions are [28]:
At $y = 0$:

$$u = u_\infty = \frac{V_f x}{l^2}, \quad (5)$$

$$T = T_w, v = 0, C = C_w,$$

and,

$$u \rightarrow 0, T \rightarrow T_\infty, C \rightarrow C_\infty \text{ as } y \rightarrow \infty \quad (6)$$

For the proposed problem, alternate geometries are obtainable through following cases:

Case 1: Plate- $m = 1=0$ and $\gamma = 0$;

Case 2: Cone- $m = 1$ and $\gamma \neq 0$;

Case 3: Wedge- $m = 0$ and $\gamma \neq 0$;

The similarities introduced are as follows:

$$\begin{aligned}\eta &= \frac{y}{l}, u = \frac{v_f x}{l^2} f', v = -\frac{v_f(m+1)}{l} f, \\ T &= (T_w - T_\infty) \theta + T_\infty, \chi = \frac{C - C_\infty}{C_w - C_\infty}\end{aligned}\quad (7)$$

Here, (u, v) are the velocity components along (x, y) directions. K^* signifies permeability of porous medium, ε_T is volumetric thermal expansion coefficient, g denotes acceleration due to gravity, (v, μ) represents fluid's kinematic viscosity and dynamic viscosity, the density and thermal conductivity of the fluid is (k, ρ) , B_0 is a uniform magnetic field, the reaction rate is K_r^2 , the modified Arrhenius function is denoted by $(T/T_\infty)^n e^{-\frac{Ea}{KT}}$ and (Ea, n) is the activation energy and fitted rate constant.

The thermophysical expressions for thermal and electrical conductivity, dynamic viscosity, density and specific heat capacity for ternary nanofluid are as follows [29]:

$$\begin{aligned}k_{tnf} &= \left(\frac{k_{S1} + 2k_{hnf} - 2\phi_1(k_{hnf} - k_{S1})}{k_{S1} + 2k_{hnf} + \phi_1(k_{hnf} - k_{S1})} \right) k_{hnf}, \\ k_{hnf} &= \left(\frac{k_{S2} + 2k_{nf} - 2\phi_2(k_{nf} - k_{S2})}{k_{S2} + 2k_{nf} + \phi_2(k_{nf} - k_{S2})} \right) k_{nf}, \\ k_{nf} &= k_f \left(\frac{k_{S3} + 2k_f - (k_f - k_{S3})2\phi_3}{k_{S3} + 2k_f + (\phi_3 k_f - \phi_3 k_{S3})} \right), \\ \sigma_{tnf} &= \left(\frac{\sigma_{S1}(1+2\phi_1) + \sigma_{hnf}(1-2\phi_1)}{\sigma_{S1}(1-\phi_1) + \sigma_{hnf}(1+\phi_1)} \right) \sigma_{hnf}, \\ \sigma_{hnf} &= \left(\frac{\sigma_{S2}(1+2\phi_2) + \sigma_{nf}(1-2\phi_2)}{\sigma_{S2}(1-\phi_2) + \sigma_{nf}(1+\phi_2)} \right) \sigma_{nf}, \\ \sigma_{nf} &= \left(\frac{\sigma_{S3}(1+2\phi_3) + \sigma_{nf}(1-2\phi_3)}{\sigma_{S3}(1-\phi_3) + \sigma_{nf}(1+\phi_3)} \right) \sigma_f. \\ \mu_{tnf} &= \frac{\mu_f}{(1-(\phi_1+\phi_2+\phi_3))^{2.5}}, \\ \rho_{tnf} &= (1-\phi_1) \left((1-\phi_2)[(1-\phi_3)\rho_f + \rho_{S3}\phi_3] + \rho_{S2}\phi_2 \right) + \rho_{S1}\phi_1,\end{aligned}$$

$$(\rho C_p)_{tnf} = \left(\frac{(\rho C_p)_{S1}\phi_1}{(\rho C_p)_f} + (1-\phi_1) \left[(1-\phi_2) \left((1-\phi_3) + \frac{(\rho C_p)_{S3}\phi_3}{(\rho C_p)_f} \right) + \frac{(\rho C_p)_{S2}\phi_2}{(\rho C_p)_f} \right] \right) (\rho C_p)_f.$$

In the above expressions, (ϕ_1, ϕ_2, ϕ_3) are solid volume fractions of copper, SWCNT and MWCNT nanoparticles respectively. And subscripts are f , nf , hnf , tnf denotes base fluid, nanofluid, hybrid nanofluid, and ternary nanofluid, and S_1, S_2, S_3 are solid particles of copper, SWCNT and MWCNT. The thermophysical properties of base fluid and nanoparticles are given in Table 1 [30].

Table 1. Thermophysical properties base fluid and ternary nanoparticles

Base Fluid and Ternary Nanoparticles	Thermophysical Properties			
	$\rho(kg/m^3)$	$Cp(J/kg/K)$	$k(W/mK)$	$\sigma(S/m)$
Water ($Pr = 6.2$)	997.1	4179	0.613	0.05
Copper (Cu)	8933	385	400	5.96×10^7
SWCNT	2600	425	6600	6.2×10^7
MWCNT	1600	796	3000	2.9×10^6

The abbreviated equations are obtained as:

$$\begin{aligned}\frac{f'''}{B_1 B_2} + (1+m)f''f - (f')^2 + \frac{Gr\theta \cos \gamma}{B_2} - \frac{\lambda f'}{B_1 B_2} \\ - Mf' = 0\end{aligned}\quad (8)$$

$$\frac{B_4}{B_3} \frac{\theta''}{Pr \frac{Ni}{B_3} \frac{1}{B_1 B_2} \frac{(\sigma_{tnf}/\sigma_f)^2}{B_3}} \quad (9)$$

$$\chi'' + Sc(m+1)f\chi' - Rc Sc(1+\delta\theta)^n e^{-\frac{E}{(1+\delta\theta)}} \chi = 0 \quad (10)$$

and

$$f' = 1, f = 0, \theta = 1, \chi = 1 \text{ at } \eta = 0, \quad (11)$$

$$f'(\infty) = 0, \theta(\infty) = 0, \chi(\infty) = 0 \text{ as } \eta \rightarrow \infty \quad (12)$$

where,

$$\begin{aligned}B_1 &= (1 - \phi_1 - \phi_2 - \phi_3)^{2.5}, \\ B_2 &= (1 - \phi_1)^{2.5} \left((1 - \phi_2) \left[(1 - \phi_3) + \frac{\rho_{S3}}{\rho_f} \phi_3 \right] + \frac{\rho_{S2}}{\rho_f} \phi_2 \right) + \frac{\rho_{S1}}{\rho_f} \phi_1, \\ B_3 &= \left(\frac{(\rho C_p)_{S1}\phi_1}{(\rho C_p)_f} + (1 - \phi_1) \left[(1 - \phi_2) \left\{ (1 - \phi_3) + \frac{(\rho C_p)_{S3}\phi_3}{(\rho C_p)_f} \right\} + \frac{(\rho C_p)_{S2}\phi_2}{(\rho C_p)_f} \right] \right), \\ B_4 &= k_{tnf} / k_f,\end{aligned}$$

and the dimensionless parameters are

$$M = \frac{\sigma_f B_0^2}{\rho_f v_f} l^2 \text{ is magnetic field parameter,}$$

$$\text{Grashof number is } Gr = \frac{g \varepsilon_T (T - T_\infty)}{u_w v_f} l^2,$$

$$\lambda = \frac{l^2}{K^*} \text{ is the permeable parameter,}$$

$$Pr = \frac{v_f(\rho C_p)}{k} \text{ is the Prandtl number,}$$

$$Ni = \frac{ql^2}{(\rho C_p)v_f} \text{ is the HSS parameter,}$$

$$Ec = \frac{u_w^2}{Cp(T - T_\infty)} \text{ is the Eckert number,}$$

$$Sc = \frac{v_f}{D_B} \text{ is the Schimdt number,}$$

$$Rc = \frac{k_f^2 l^2}{v_f} \text{ is the reaction rate parameter,}$$

$$\text{and the temperature difference is denoted by } \delta = \frac{T_w - T_\infty}{T_\infty}.$$

With suitable similarity transformations, the significant physical parameters such as Cf_x -Skin friction, Nu_x -Nusselt number, and Sh_x -Sheerwood number are given as follows:

$$\begin{aligned}Cf_x &= \frac{\tau_w}{\rho_f u_w^2}, \quad Nu_x = \frac{l q_w}{k_f (T_w - T_\infty)}, \text{ and} \\ Sh_x &= \frac{l r_w}{D_B (C_w - C_\infty)}\end{aligned}\quad (13)$$

where,

$$\begin{aligned}\tau_w &= \mu_{mf} \frac{\partial u}{\partial y} \Big|_{y=0}, \quad q_w = -k_{mf} \frac{\partial T}{\partial y} \Big|_{y=0}, \text{ and} \\ r_w &= -D_B \frac{\partial C}{\partial y} \Big|_{y=0}\end{aligned}\quad (14)$$

Upon replacing Eq. (14) into Eq. (13), we possess

$$\begin{aligned}\frac{l}{x} Cf &= f''(0), \quad Nu = -\left(k_{mf}/k_f\right)\theta'(0), \text{ and} \\ Sh &= -\chi'(0)\end{aligned}\quad (15)$$

3. NUMERICAL PROCEDURE

The shooting method and RKF-45 technique was used to resolve the gained Eqs. (8)-(10) and to deduce the BCs. Initially, we transform the obtained equations into first order framework.

So, consider

$$f = r_1, f' = r_2, f'' = r_3, \theta = r_4, \theta' = r_5, \chi = r_6, \chi' = r_7 \quad (16)$$

From this we obtain,

$$r_3^1 = -(B_1 B_2) * ((m + 1) * r_1 * r_3 - r_2^2 + (Gr * r_4 * \cos\gamma)/B_2 - (\lambda/B_1 B_2) * r_2 - M * r_2) \quad (17)$$

$$\begin{aligned}r_5' &= -\frac{(B_3 * k_f * Pr)}{k_{tnf}} * ((m + 1) * r_1 * r_5 + \frac{(Ni)}{B_3} * r_4 + \frac{(Ec)}{B_1 B_3} * r_3^2 + \frac{(\sigma_{tnf}/\sigma_f)}{B_3} * M * Ec * r_2^2) \quad (18)\end{aligned}$$

and,

$$r_7' = -Sc * ((m + 1) * r_1 * r_7 - Rc * (1 + \delta * r_4)^n * \exp(-E/(1 + \delta * r_4)) * r_6) \quad (19)$$

Also, the BCs. becomes

$$\left. \begin{aligned}r_2(0) &= 1, r_1(0) = 0, r_4(0) = 1, r_6(0) = 1 \\ r_2(\infty) &= 0, r_4(\infty) = 0, r_6(\infty) = 0\end{aligned} \right\} \quad (20)$$

Using the help of RKF-45 method, the initial value problem (IVP) in Eqns. (16-20) is resolved numerically and with the assistance of shooting technique the unknown values are obtained by passing on step size and tolerance error to be $h = 0.01$ and 10^{-6} respectively, also satisfying the boundary conditions at infinite level. The numerical were gained utilizing the bvp4c algorithm. For computational simulations we have fixed ranges of parameters as $M = 0.5, 1, 1.5$, $Gr = 1$, $Ni = Rc = 0.5$, $Sc = 0.6$, $Ec = 0.1$, $n = \delta = E = 0.1$. Moreover, the numerical results of present study are compared to those of previous studies, it was found results were similar, see Table 2 and Table 3.

Table 2. Code validation for $-f''(0)$ at several values of Pr when $m = Gr = M = \phi_1 = \phi_2 = \phi_3 = 0$

λ	Kameswaran et al. [31]	Present Study (RKF-45)
0.5	1.22474487	1.22474636
1.0	1.41421356	1.41421532
1.5	1.58113883	1.58114100
2.0	1.73205081	1.73205641
5	2.44948974	2.44949213

Table 3. Code validation for $-\theta'(0)$ at different values of Pr when $m = Ec = M = Ni = \phi_1 = \phi_2 = \phi_3 = 0$

Pr	Salleh et al. [32]	Present Study (RKF-45)
0.72	0.46317	0.46350
1	0.58198	0.58210
3	1.16522	1.16526
5	1.56806	1.56812
7	1.89548	1.89543
10	2.30821	2.30817
100	7.76249	7.76253

4. ANALYSIS OF RESULTS

This section discusses the primary outcome of the current effort. The resulting solutions for various non-dimensional parameters are shown using appropriate profiles. Several parameter values were chosen to describe the behaviours of the heat transfer and flow dynamics characteristics. In this case, the current problem includes various relevant parameters such as magnetic field M , permeability parameter λ , Grashof number Gr , Eckert number Ec , HSS parameter Ni , reaction rate parameter Rc , and activation energy parameter E . In addition to this, the effects of some of these parameters on Skin-friction, Nusselt number, and Sherwood number, are depicted in graphs and tables. All the graphs are plotted for cone (Dash lines), wedge (solid lines), and plate (dot lines) for better comparison of results. Figures 2-4 represent the deviations of M , λ , Gr over velocity profile for three different fluid flow cases. Figure 2 explains that on increasing M there is reduction in the movement of fluid particles resulting in the decreasing of fluid velocity in all three cases.

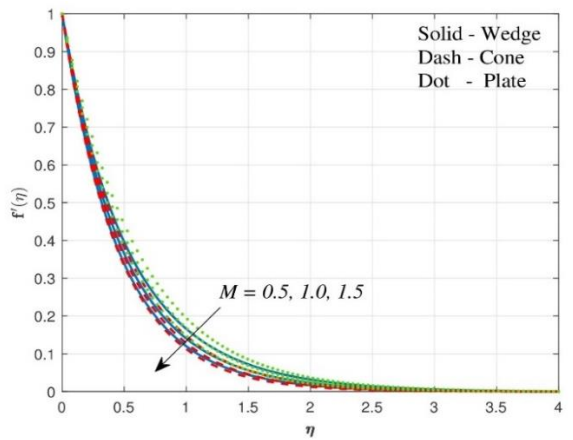


Figure 2. $f'(\eta)$ curves for varying M

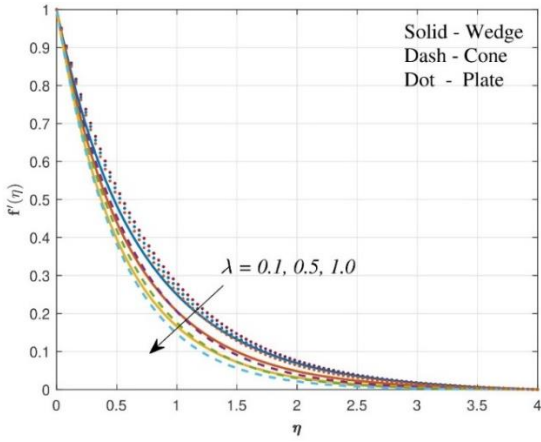


Figure 3. $f'(\eta)$ curves for varying λ

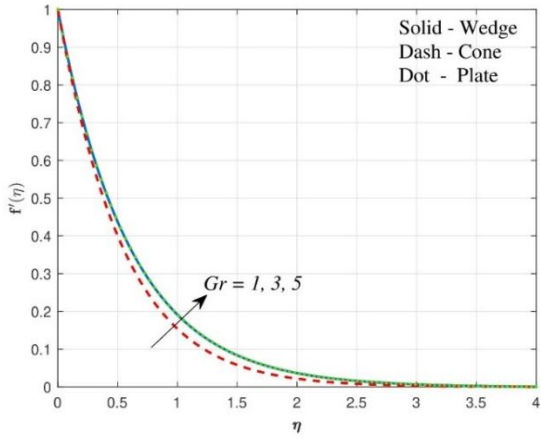


Figure 4. $f'(\eta)$ curves for varying Gr

From the Figure 2 it is evident that f' for flow across cone declines faster than in the remaining cases. In Figure 3 it is seen that rise in the value of λ diminishes f' for all flow cases. It is due to fact the rise in the λ increases system's resistance.

As a result of developed force of friction, the flow velocity is reduced. Further, curves of $f'(\eta)$ for flow past cone lessens faster than in remaining cases. The escalate in the $f'(\eta)$ profile for upsurge values of Gr for all flow cases is displayed in the Figure 4. From physical standpoint increased Gr values reduce thickness of boundary layer due to buoyant forces produced by fluctuations in temperature. Besides, the $f'(\eta)$ for the fluid flow over plate proliferates quicker than in any other cases.

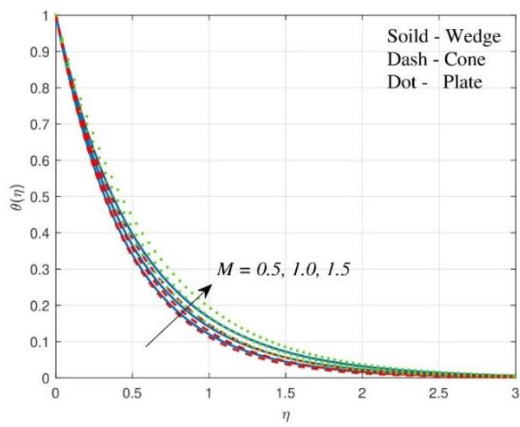


Figure 5. $\theta(\eta)$ curves for different M values

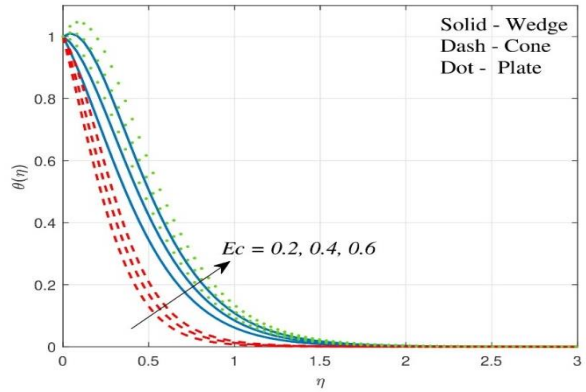


Figure 6. $\theta(\eta)$ curves for different Ec values

Figure 5 displays the escalating nature in thermal gradient profile for M in all fluid flow cases. Since increasing magnetic field creates fluid resistance to flow which intern facilitates upsurge in thermal distribution. It is witnessed that thermal distribution is more in plate when compared with left cases. The effect of Eckert number over $\theta(\eta)$ is exhibited in Figure 6.

Here, an increase in the Ec promotes rise in $\theta(\eta)$. Physically, a spike in the Ec thickens thermal boundary layer and moreover this effect is more pronounced in the presence of magnetic field. The behaviours of Ni parameter over $\theta(\eta)$ for all flow cases is studied in Figure 7. Furthermore, the fluid flow past wedge unveils better heat transference than in left over cases. Internal heat sink/source (HSS) hinders or facilitates heat transfer. As we magnify impact of Ni thickness of $\theta(\eta)$ increases. Better heat transfer will be seen when we rise HSS values from negative to positive and also the occurrence of a heat source stimulates the fluid's temperature. As a result, as heat is absorbed, and with buoyancy's effect boosts the flow and enhances heat transmission. Figure 8 demonstrate the influence of Rc over $\chi(\eta)$ for all flow cases. In all flow cases, it is evident that increase in Rc descends $\chi(\eta)$. This is because, when the reaction rate parameter is raised, the concentration of the entire fluid medium diminutions due to lower mass diffusivity and also due to the fact that lot of chemical consumption takes place during chemical reaction. A lower mass transfer rate is perceived in fluid flow across cone. Figure 9 shows the effect of E on $\chi(\eta)$ for all flow cases. The growth in the E value stimulates $\chi(\eta)$. Increasing E values reduce the Arrhenius process, thereby elevating the rate of the generative chemical process that generates concentration. More enhancement in the concentration is observed in fluid flow case over plate.

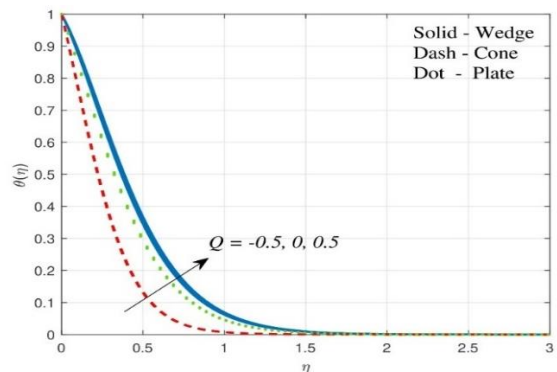


Figure 7. $\theta(\eta)$ curves for different Q values

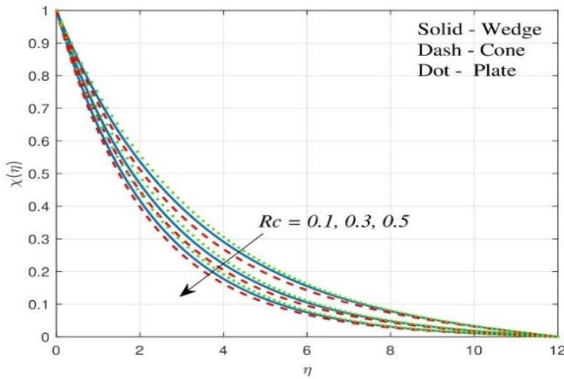


Figure 8. $\chi(\eta)$ curves for distinct Rc values

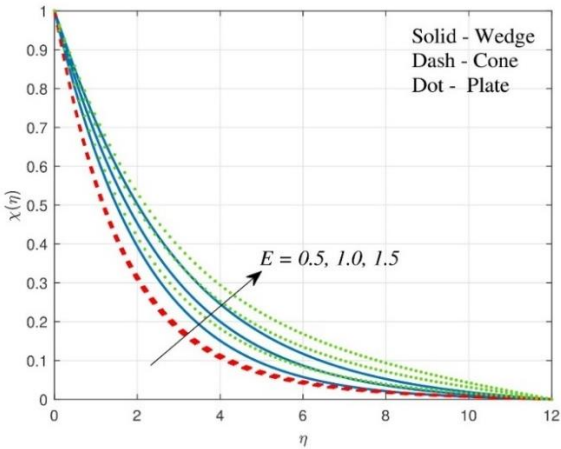


Figure 9. $\chi(\eta)$ curves for distinct E values

Figure 10 shows the variations in the values of Cfx for various values of λ and Gr for all three flow cases. In general, the existence of a porous media increases skin friction. This is because the flow through the porous media involves viscous dissipation within the pores, resulting in greater shear stress at the solid surface, and skin friction doubles with a surge in the Grashof number due to a raise in the velocity distribution. Hence it is portrayed that skin-friction increases for λ and Gr . Additionally, compared to the other circumstances, skin friction is improved in the fluid flow case through cone. Effect of skin friction is studied in the design of aircrafts, ships, and other automobiles that move through fluids. Figure 11 illustrates how the increasing value of ϕ over Nu_x versus Q for all three fluid flow cases.

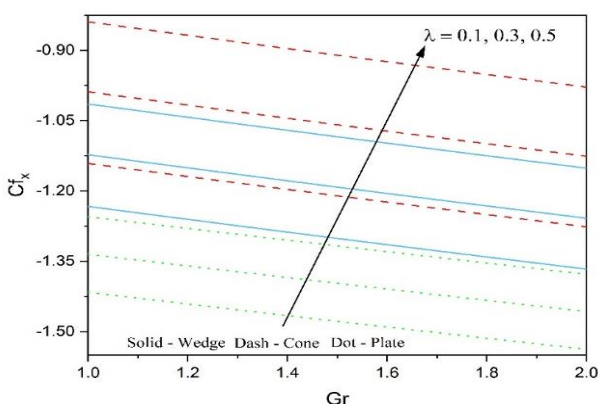


Figure 10. Influence of (λ, Gr) over Skin-friction Cfx

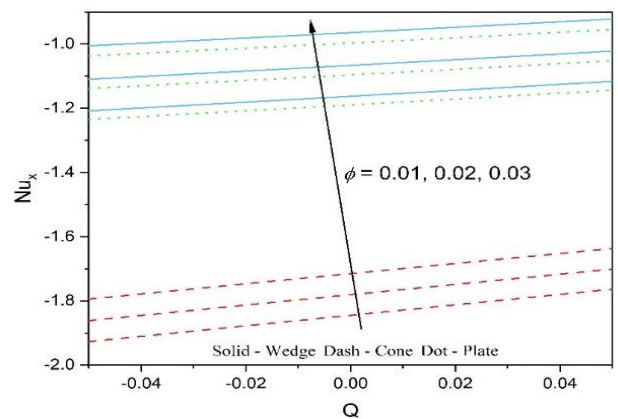


Figure 11. Influence of (ϕ, Q) over Nusselt number Nu_x

In general, a rise in the solid volume fraction corresponds to an increase in the Nusselt number. This is due to the fact that as the solid volume fraction increases, so does the heat transfer coefficient and so does the Nusselt number of nanoparticles and also presence of Q promotes heat transfer across boundary layer. However, in the case of flow across wedge, an enriched heat transmission rate is observed. Analysis of Nusselt number is a significant due to its wide range of industrial applications such as cooling systems, chemical and aerospace engineering. Figure 12 presents the decreasing behaviour Sherwood number under the impacts of E . The activation energy may impact the concentration distribution and mass transfer rate, which in turn can affect the Sherwood number. A higher activation energy may result in a lower mass transfer rate, and thus a lower Sherwood number. In biomedical engineering analysis of Sherwood number is important to design and optimize drug delivery systems and much more.

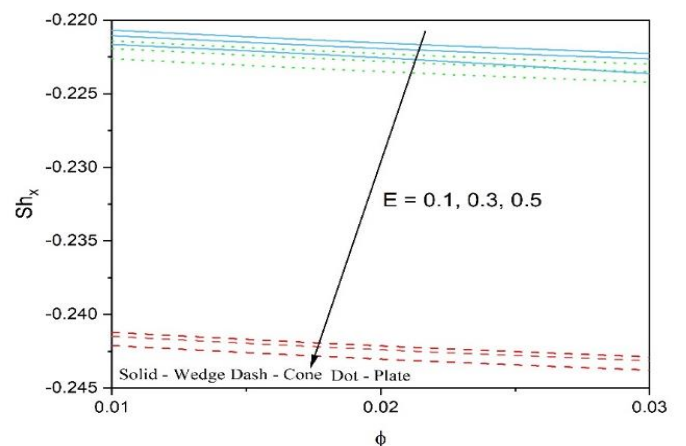


Figure 12. Influence of (E, ϕ) over Sherwood number Sh_x

5. CONCLUSIONS

In this research, the MHD ternary nanofluid flow past three different geometries is investigated in the presence of joule heating, viscous dissipation, HSS, activation energy, and chemical reaction. A visual examination of the behavior of the effective concentration, thermal gradient, and velocity profiles for various parameters is performed graphically. Also, through graphs the skin-friction and heat and mass transfer rates are

discussed in three fluid flow cases. The following is a summary of the core conclusions of this current research.

(1) The $f'(\eta)$ curves for fluid flow across plate drops quicker for varying M and λ values than in other cases.

(2) The rising values of Gr accelerates the fluid flow and it is evident from the graph that the increase in $f'(\eta)$ is slightly higher in plate when compared to other geometries.

(3) The heat transfer in all three fluid cases has improved for growing Ec and Q parametric values.

(4) The $\chi(\eta)$ curves for fluid flow over cone has dropped more than in other cases due to augmented values of Rc values.

(5) The activation energy (E) has a positive impact over $\chi(\eta)$ hence $\chi(\eta)$ curves an increasing behaviour is observed in all fluid flow cases for elevated values of E . Moreover, we noticed that the mass transfer is higher in plate than in other scenarios.

(6) The augmented ϕ values have enhanced the heat transmission rate for all three fluid flow cases. Furthermore, increased heat transfer is noticed in fluid flow case over wedge than in other two cases.

ACKNOWLEDGEMENT

This work is funded by the Grant NRF2022-R1A2C2002799 of the National Research Foundation of Korea.

REFERENCES

- [1] Abbasi, A., Ashraf, W. (2023). Analysis of heat transfer performance for ternary nanofluid flow in radiated channel under different physical parameters using GFEM. *Journal of the Taiwan Institute of Chemical Engineers*, 146: 104887. <https://doi.org/10.1016/j.jtice.2023.104887>
- [2] Animasaun, I.L., Al-Mdallal, Q.M., Khan, U., Alshomrani, A.S. (2022). Unsteady water-based ternary hybrid nanofluids on wedges by bioconvection and wall stretching velocity: Thermal analysis and scrutinization of small and larger magnitudes of the thermal conductivity of nanoparticles. *Mathematics*, 10(22): 4309. <https://doi.org/10.3390/math10224309>
- [3] Maranna, T., Mahabaleshwar, U.S., Perez, L.M., Manca, O. (2023). Flow of viscoelastic ternary nanofluid over a shrinking porous medium with heat Source/Sink and radiation. *Thermal Science and Engineering Progress*, 40: 101791. <https://doi.org/10.1016/j.tsep.2023.101791>
- [4] Alanazi, M.M., Ahmed Hendi, A., Ahammad, N.A., Ali, B., Majeed, S., Shah, N.A. (2023). Significance of ternary hybrid nanoparticles on the dynamics of nanofluids over a stretched surface subject to gravity modulation. *Mathematics*, 11(4): 809. <https://doi.org/10.3390/math11040809>
- [5] Gamiel, Y., Elbehairy, M., El-Sayed, M.K. (2022). Impact of a transverse magnetic field on flow through porous cylindrical fiber beds with permeability enhancement analysis. *Alexandria Engineering Journal*, 61(11): 8667-8675. <https://doi.org/10.1016/j.aej.2022.02.003>
- [6] Fetecau, C., Moroşanu, C. (2023). Influence of magnetic field and porous medium on the steady state and flow resistance of second grade fluids over an infinite plate. *Symmetry*, 15(6): 1269. <https://doi.org/10.3390/sym15061269>
- [7] Manjunatha, N., Abdulrahman, A., Khan, U., Sumithra, R., Gill, H.S., Elattar, S., Eldin, S.M. (2023). Triple diffusive Marangoni convection in a fluid-porous structure: Effects of a vertical magnetic field and temperature profiles. *Case Studies in Thermal Engineering*, 43: 102765. <https://doi.org/10.1016/j.csite.2023.102765>
- [8] Mahabaleshwar, U.S., Nagaraju, K.R., Kumar, P.V., Nadagouda, M.N., Bennacer, R., Sheremet, M.A. (2020). Effects of dufour and soret mechanisms on MHD mixed convective-radiative non-newtonian liquid flow and heat transfer over a porous sheet. *Thermal Science and Engineering Progress*, 16: 100459. <https://doi.org/10.1016/j.tsep.2019.100459>
- [9] Aslani, K.E., Mahabaleshwar, U.S., Singh, J., Sarris, I.E. (2021). Combined effect of radiation and inclined MHD flow of a micropolar fluid over a porous stretching/shrinking sheet with mass transpiration. *International Journal of Applied and Computational Mathematics*, 7: 1-21. <https://doi.org/10.1007/s40819-021-00987-7>
- [10] Jayanthi, S., Niranjan, H. (2023). Effects of joule heating, viscous dissipation, and activation energy on nanofluid flow induced by MHD on a vertical surface. *Symmetry*, 15(2): 314. <https://doi.org/10.3390/sym15020314>
- [11] Naseem, T., Fatima, U., Munir, M., Shahzad, A., Kausar, N., Nisar, K.S., Saleel, C.A., Abbas, M. (2022). Joule heating and viscous dissipation effects in hydromagnetized boundary layer flow with variable temperature. *Case Studies in Thermal Engineering*, 35: 102083. <https://doi.org/10.1016/j.csite.2022.102083>
- [12] Yashkun, U., Zaimi, K., Ishak, A., Pop, I., Sidaoui, R. (2021). Hybrid nanofluid flow through an exponentially stretching/shrinking sheet with mixed convection and Joule heating. *International Journal of Numerical Methods for Heat & Fluid Flow*, 31(6): 1930-1950. <https://doi.org/10.1108/HFF-07-2020-0423>
- [13] Khashi'e, N.S., Arifin, N.M., Pop, I. (2022). Magnetohydrodynamics (MHD) boundary layer flow of hybrid nanofluid over a moving plate with Joule heating. *Alexandria Engineering Journal*, 61(3): 1938-1945. <https://doi.org/10.1016/j.acj.2021.07.032>
- [14] Sajid, T., Jamshed, W., Eid, M.R., Altamirano, G.C., Aslam, F., Alanzi, A.M., Abd-Elmonem, A. (2023). Magnetized cross tetra hybrid nanofluid passed a stenosed artery with nonuniform heat source (sink) and thermal radiation: Novel tetra hybrid Tiwari and Das nanofluid model. *Journal of Magnetism and Magnetic Materials*, 569: 170443. <https://doi.org/10.1016/j.jmmm.2023.170443>
- [15] Vajravelu, K., Hadjinicolaou, A. (1993). Heat transfer in a viscous fluid over a stretching sheet with viscous dissipation and internal heat generation. *International Communications in Heat and Mass Transfer*, 20(3): 417-430. [https://doi.org/10.1016/0735-1933\(93\)90026-R](https://doi.org/10.1016/0735-1933(93)90026-R)
- [16] Chen, C.H. (2006). Effect of viscous dissipation on heat transfer in a non-Newtonian liquid film over an unsteady stretching sheet. *Journal of Non-Newtonian Fluid Mechanics*, 135(2-3): 128-135. <https://doi.org/10.1016/j.jnnfm.2006.01.009>

- [17] Mahesh, R., Mahabaleshwar, U.S., Kumar, P.V., Öztop, H.F., Abu-Hamdeh, N. (2023). Impact of radiation on the MHD couple stress hybrid nanofluid flow over a porous sheet with viscous dissipation. *Results in Engineering*, 17: 100905. <https://doi.org/10.1016/j.rineng.2023.100905>
- [18] Hassan, A., Hussain, A., Arshad, M., Gouadria, S., Awrejcewicz, J., Galal, A.M., Alharbi, F.M., Eswaramoorthi, S. (2022). Insight into the significance of viscous dissipation and heat generation/absorption in magneto-hydrodynamic radiative casson fluid flow with first-order chemical reaction. *Frontiers in Physics*, 605. <https://doi.org/10.3389/fphy.2022.920372>
- [19] Masood, S., Farooq, M., Ahmad, S. (2020). Description of viscous dissipation in magnetohydrodynamic flow of nanofluid: Applications of biomedical treatment. *Advances in Mechanical Engineering*, 12(6): 1687814020926359. <https://doi.org/10.1177/1687814020926359>
- [20] Zaib, A., Rashidi, M.M., Chamkha, A.J., Mohammad, N.F. (2018). Impact of nonlinear thermal radiation on stagnation-point flow of a Carreau nanofluid past a nonlinear stretching sheet with binary chemical reaction and activation energy. *Proceedings of the Institution of Mechanical Engineers, Part C: Journal of Mechanical Engineering Science*, 232(6): 962-972. <https://doi.org/10.1177/0954406217695847>
- [21] Mustafa, M., Khan, J.A., Hayat, T., Alsaedi, A. (2017). Buoyancy effects on the MHD nanofluid flow past a vertical surface with chemical reaction and activation energy. *International Journal of Heat and Mass Transfer*, 108: 1340-1346. <https://doi.org/10.1016/j.ijheatmasstransfer.2017.01.029>
- [22] Ijaz, M., Ayub, M., Malik, M.Y., Khan, H., Alderremy, A.A., Aly, S. (2020). Entropy analysis in nonlinearly convective flow of the Sisko model in the presence of Joule heating and activation energy: The Buongiorno model. *Physica Scripta*, 95(2): 025402. <https://doi.org/10.1088/1402-4896/ab2dc7>
- [23] Bhatti, M.M., Michaelides, E.E. (2021). Study of Arrhenius activation energy on the thermo-bioconvection nanofluid flow over a Riga plate. *Journal of Thermal Analysis and Calorimetry*, 143: 2029-2038. <https://doi.org/10.1007/s10973-020-09492-3>
- [24] Jabeen, K., Mushtaq, M., Mushtaq, T., Muntazir, R.M.A. (2023). A numerical study of boundary layer flow of Williamson nanofluid in the presence of viscous dissipation, bioconvection, and activation energy. *Numerical Heat Transfer, Part A: Applications*, 1-22. <https://doi.org/10.1080/10407782.2023.2187494>
- [25] Vajravelu, K., Nayfeh, J. (1992). Hydromagnetic convection at a cone and a wedge. *International Communications in Heat and Mass Transfer*, 19(5): 701-710. [https://doi.org/10.1016/0735-1933\(92\)90052-J](https://doi.org/10.1016/0735-1933(92)90052-J)
- [26] Prabakaran, R., Eswaramoorthi, S., Loganathan, K., Sarris, I.E. (2022). Investigation on thermally radiative mixed convective flow of carbon nanotubes/Al₂O₃ nanofluid in water past a stretching plate with joule heating and viscous dissipation. *Micromachines*, 13(9): 1424. <https://doi.org/10.3390/mi13091424>
- [27] Khan, W.A., Sultan, F., Ali, M., Shahzad, M., Khan, M., Irfan, M. (2019). Consequences of activation energy and binary chemical reaction for 3D flow of cross-nanofluid with radiative heat transfer. *Journal of the Brazilian Society of Mechanical Sciences and Engineering*, 41: 1-13. <https://doi.org/10.1007/s40430-018-1482-0>
- [28] Ali, M.E., Sandeep, N. (2017). Cattaneo-Christov model for radiative heat transfer of magnetohydrodynamic Casson-ferrofluid: A numerical study. *Results in Physics*, 7: 21-30. <https://doi.org/10.1016/j.rinp.2016.11.055>
- [29] Wang, F., Nazir, U., Sohail, M., El-Zahar, E.R., Park, C., Thounthong, P. (2022). A Galerkin strategy for tri-hybridized mixture in ethylene glycol comprising variable diffusion and thermal conductivity using non-Fourier's theory. *Nanotechnology Reviews*, 11(1): 834-845. <https://doi.org/10.1515/ntrev-2022-0050>
- [30] Othman, M.N., Jedi, A., Bakar, N.A.A. (2021). MHD flow and heat transfer of hybrid nanofluid over an exponentially shrinking surface with heat source/sink. *Applied Sciences*, 11(17): 8199. <https://doi.org/10.3390/app11178199>
- [31] Kameswaran, P.K., Shaw, S., Sibanda, P.V.S.N., Murthy, P.V.S.N. (2013). Homogeneous-heterogeneous reactions in a nanofluid flow due to a porous stretching sheet. *International Journal of Heat and Mass Transfer*, 57(2): 465-472. <https://doi.org/10.1016/j.ijheatmasstransfer.2012.10.047>
- [32] Salleh, M.Z., Nazar, R., Pop, I. (2010). Boundary layer flow and heat transfer over a stretching sheet with Newtonian heating. *Journal of the Taiwan Institute of Chemical Engineers*, 41(6): 651-655. <https://doi.org/10.1016/j.jtice.2010.01.013>